

Thermodynamic bound on heat to power conversion

Rongxiang Luo,¹ Giuliano Benenti,^{2,3,4} Giulio Casati,^{2,5} and Jiao Wang¹

¹*Department of Physics, Key laboratory of Low Dimensional Condensed Matter Physics (Department of Education of Fujian Province), and Jiujiang Research Institute, Xiamen University, Xiamen 361005, Fujian, China*

²*Center for Nonlinear and Complex Systems, Dipartimento di Scienza e Alta Tecnologia, Università degli Studi dell'Insubria, via Valleggio 11, 22100 Como, Italy*

³*Istituto Nazionale di Fisica Nucleare, Sezione di Milano, via Celoria 16, 20133 Milano, Italy*

⁴*NEST, Istituto Nanoscienze-CNR, I-56126 Pisa, Italy*

⁵*International Institute of Physics, Federal University of Rio Grande do Norte, Campus Universitário - Lagoa Nova, CP. 1613, Natal, Rio Grande Do Norte 59078-970, Brazil*

In systems described by the scattering theory, there is an upper bound, lower than Carnot, on the efficiency of steady-state heat to work conversion at a given output power. We show that interacting systems can overcome such bound and saturate, in the thermodynamic limit, the much more favorable linear-response bound. This result is rooted in the possibility for interacting systems to achieve the Carnot efficiency at the thermodynamic limit without delta-energy filtering, so that large efficiencies can be obtained without greatly reducing power.

PACS numbers: 05.70.Ln

Introduction. The increasing energy demand and the depletion and environmental impact of fossil fuels calls for renewable and eco-friendly energy resources. In this frame, nanoscale thermal engines [1–12] will play an important role and might become part of the energetic mix of the future. A crucial point is the efficiency of such engines. Given any heat engine operating between two reservoirs at temperature T_L and T_R ($T_L > T_R$), the efficiency of energy conversion is upper bounded by the Carnot efficiency $\eta_C = 1 - T_R/T_L$. This limit can be achieved for dissipationless heat engines. Such ideal machines operate reversibly and infinitely slowly, and therefore the extracted power vanishes in the Carnot limit. For any practical purpose it is therefore crucial to consider the *power-efficiency trade-off*, in order to design devices that work at the maximum possible efficiency for a given output power.

For steady-state conversion of heat to work in quantum systems which can be modelled by the Landauer-Büttiker scattering theory, this problem was solved theoretically by Whitney [13, 14]. Indeed, he found a bound on the efficiency at a given output power P , which equals the Carnot efficiency at $P = 0$, and decays with increasing P . This upper bound is achieved when only particles within a given energy window (determined by the desired output power P) of width $\delta(P)$ can be transmitted through the system. The Carnot efficiency is obtained for delta-energy filtering [15–17], that is, when $\delta \rightarrow 0$, and in such limit the output power vanishes. This interesting result establishes a bound for an important class of systems. Now the relevant question is: how general is this bound? For general interacting systems, can this bound be overcome, thus allowing for a better power-efficiency trade-off?

In this letter, we give a positive answer to this question for classical systems. Indeed, we show that interact-

ing, nonintegrable momentum-conserving systems, overcome the bound from the scattering theory. These systems can achieve the Carnot efficiency at the thermodynamic limit, with a much more favorable power-efficiency trade-off than allowed by the scattering theory. Therefore, interactions can significantly improve the performance of steady-state heat to work conversion. This result is rooted in the possibility, for interacting systems, to achieve the Carnot efficiency without delta-energy filtering. Our results are illustrated by means of extensive numerical simulations of classical models of elastically colliding particles.

Classical reservoirs. For concreteness, we consider a one-dimensional system (even though, as discussed in the conclusions and shown in Sec. D of the supplementary material, our analysis can be extended to higher dimensions), whose ends are in contact with left/right reservoirs, characterized by temperature T_α and electrochemical potential μ_α ($\alpha = L, R$). The reservoirs are modelled as infinite one-dimensional ideal gases, with particle velocities described by the Maxwell-Boltzmann distribution, $F_\alpha(v) = \sqrt{\frac{m}{2\pi k_B T_\alpha}} \exp\left(-\frac{mv^2}{2k_B T_\alpha}\right)$, where k_B is the Boltzmann constant and m the mass of the particles. We use a stochastic model of the reservoirs [18, 19]: whenever a particle of the system crosses the boundary which separates the system from the left or right reservoir, it is removed. On the other hand, particles are injected into the system from the boundaries, with rates γ_α . The injection rate γ_α is computed by counting how many particles from reservoir α cross the reservoir-system boundary per unit time: $\gamma_\alpha = \rho_\alpha \int_0^\infty dv v F_\alpha(v) = \rho_\alpha \sqrt{\frac{k_B T_\alpha}{2\pi m}}$, with ρ_α the particle number density of the ideal gas in reservoir α . A standard derivation [20] then shows that the density ρ_α is related to the electrochemical potential μ_α as follows: $\mu_\alpha = k_B T_\alpha \ln(\rho_\alpha \lambda_\alpha)$, where $\lambda_\alpha = h/\sqrt{2\pi m k_B T_\alpha}$ is the de Broglie thermal wave length and h the Planck

constant.

Non-interacting systems. In this case, the particle current reads [20]

$$J_\rho = \gamma_L \int_0^\infty d\epsilon u_{L}(\epsilon) \mathcal{T}(\epsilon) - \gamma_R \int_0^\infty d\epsilon u_{R}(\epsilon) \mathcal{T}(\epsilon), \quad (1)$$

where $u_\alpha(\epsilon) = \beta_\alpha e^{-\beta_\alpha \epsilon}$, with $\beta_\alpha = (k_B T_\alpha)^{-1}$, is the energy distribution of the particles injected from reservoir α and $\mathcal{T}(\epsilon)$ is the transmission probability for a particle with energy ϵ to transit from one end to another of the system, $0 \leq \mathcal{T}(\epsilon) \leq 1$. We can equivalently rewrite the particle current in a form which can be seen as the classical analogue to the Landauer-Büttiker approach:

$$J_\rho = \frac{1}{h} \int_0^\infty d\epsilon [f_L(\epsilon) - f_R(\epsilon)] \mathcal{T}(\epsilon), \quad (2)$$

where $f_\alpha(\epsilon) = e^{-\beta_\alpha(\epsilon - \mu_\alpha)}$ is the Maxwell-Boltzmann distribution function. Similarly, we obtain the heat current from reservoir α as

$$J_{h,\alpha} = \frac{1}{h} \int_0^\infty d\epsilon (\epsilon - \mu_\alpha) [f_L(\epsilon) - f_R(\epsilon)] \mathcal{T}(\epsilon). \quad (3)$$

To proceed we take the reference electrochemical potential to be that of reservoir L and set $\mu_L = 0$. Following the same steps as done in Refs. [13, 14] for the quantum case, we find the transmission function that maximizes the efficiency of the heat engine, $\eta(P) = P/J_{h,L}$, for a given output power $P = (\Delta\mu)J_\rho$, with $\Delta\mu = \mu_R - \mu_L > 0$ and $P, J_{h,L} > 0$. It turns out that the optimal \mathcal{T} is a box-car function, $\mathcal{T}(\epsilon) = 1$ for $\epsilon_0 < \epsilon < \epsilon_1$ and $\mathcal{T}(\epsilon) = 0$ otherwise. Here $\epsilon_0 = \Delta\mu/\eta_C$ is obtained from the condition $f_L(\epsilon_0) = f_R(\epsilon_0)$ and ϵ_1 can be determined numerically by solving the equation $\epsilon_1 = \Delta\mu J'_{h,L}/P'$, where the prime indicates the derivative over $\Delta\mu$ for fixed \mathcal{T} (this equation is transcendental since $J_{h,L}$ and P depend on ϵ_1). The maximum achievable power (according to scattering theory) is obtained when $\epsilon_1 \rightarrow \infty$:

$$P_{\max}^{(\text{st})} = A \frac{\pi^2}{h} k_B^2 (\Delta T)^2, \quad (4)$$

where $\Delta T = T_L - T_R$ and $A \approx 0.0373$. Note that $\Delta\mu$ is determined from the above optimization procedure; in particular at $P_{\max}^{(\text{st})}$ we obtain $\Delta\mu = k_B \Delta T$. At small output power, $P/P_{\max}^{(\text{st})} \ll 1$, the upper bound on efficiency approaches the Carnot efficiency as follows:

$$\eta(P) \leq \eta_{\max}^{(\text{st})}(P) = \eta_C \left(1 - B \sqrt{\frac{T_R}{T_L} \frac{P}{P_{\max}^{(\text{st})}}} \right), \quad (5)$$

where $B \approx 0.493$. In the limit $\epsilon_1 \rightarrow \infty$, $P \rightarrow 0$ and $\eta \rightarrow \eta_C$. In this case, we recover the well-known delta-energy filtering mechanism to achieve the Carnot efficiency [15–17]. Namely, we recover the Carnot limit when transmission is possible only inside an energy window of

width $\delta = \epsilon_1 - \epsilon_0 \rightarrow 0$. It is intuitive that selecting transmission over a tiny energy window greatly reduces power production. It is therefore natural to expect that a different mechanism to reach Carnot efficiency might allow a larger power production. Indeed in what follows we show that for interacting, momentum-conserving systems, where the Carnot efficiency can be reached without delta-energy filtering (see Sec. C in the supplementary material), a greatly improved power-efficiency trade-off can be obtained.

Momentum-conserving systems. We consider a system of elastically colliding particles, in contact with two reservoirs tuned at different temperatures and electrochemical potentials in order to maintain a steady flow of particles and heat. The equations connecting fluxes and thermodynamic forces within linear response (an approximation that we will show later to be valid for our model) are [21, 22]

$$\begin{pmatrix} J_\rho \\ J_u \end{pmatrix} = \begin{pmatrix} L_{\rho\rho} & L_{\rho u} \\ L_{u\rho} & L_{uu} \end{pmatrix} \begin{pmatrix} -\nabla(\beta\mu) \\ \nabla\beta \end{pmatrix}, \quad (6)$$

where J_ρ is the steady particle current, J_u is the steady energy current, and L_{ij} (with $i, j = \rho, u$) are the kinetic (Onsager) coefficients. Hereafter we will discuss our results in the language of thermoelectricity, even though they could equally well refer to other steady-state heat to work conversion phenomena like thermodiffusion. The Onsager coefficients are then related to the familiar transport coefficients as follows:

$$\sigma = \frac{e^2}{T} L_{\rho\rho}, \quad \kappa = \frac{1}{T^2} \frac{\det \mathbb{L}}{L_{\rho\rho}}, \quad S = \frac{1}{eT} \left(\frac{L_{\rho u}}{L_{\rho\rho}} - \mu \right). \quad (7)$$

Here σ is the electrical conductivity, κ is the thermal conductivity, and S is the thermopower; Besides, e is the charge of the conducting particles, $T \approx T_L \approx T_R$ and $\mu \approx \mu_L \approx \mu_R$ in the linear response formulas, and $\det \mathbb{L}$ denotes the determinant of the (Onsager) matrix of kinetic coefficients. Thermodynamics imposes $\det \mathbb{L} \geq 0$, $L_{\rho\rho} \geq 0$, $L_{uu} \geq 0$, and the Onsager reciprocity relations ensure (for systems with time-reversal symmetry) that $L_{u\rho} = L_{\rho u}$. The maximum efficiency for energy conversion achievable by the system is a monotonically growing function of the thermoelectric figure of merit ZT [12]:

$$ZT = \frac{\sigma S^2}{\kappa} T = \frac{(L_{u\rho} - \mu L_{\rho\rho})^2}{\det \mathbb{L}}. \quad (8)$$

Thermodynamics imposes $ZT \geq 0$, with the efficiency $\eta = 0$ when $ZT = 0$ and $\eta \rightarrow \eta_C$ when $ZT \rightarrow \infty$.

Hereafter, we illustrate the breaking of bound (5) by considering a one-dimensional, diatomic chain of hard-point elastically colliding particles connected to reservoirs, with masses $m_i \in \{m, M\}$ and $m \neq M$. (See [20] for details of the model.) We have performed a nonequilibrium calculation of the transport coefficients and then

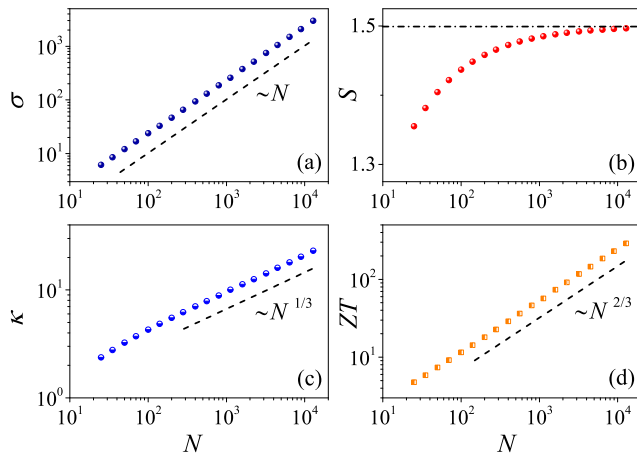


FIG. 1. Electrical conductivity σ (a), thermopower S (b), thermal conductivity κ (c) and figure of merit ZT (d) as a function of the mean number N of particles inside the system, for the one-dimensional, diatomic hard-point gas. Here and in the other figures, the data are obtained for $M = 3$, $T = 1$, and $\mu = 0$.

of the figure of merit ZT (we have developed a method to determine very accurately the transport coefficients, see the supplementary material, Sec. B, for details). In our simulations, we set $k_B = m = e = 1$ and the system length, L , to be equal to the mean number of particles, N , inside the system. Our data shown in Fig. 1 as well as theoretical arguments [23] show that the electrical conductivity $\sigma \propto N$, the thermal conductivity $\kappa \propto N^\xi$, with the power $\xi = 1/3$ predicted by hydrodynamics approach [24, 25], the thermopower is asymptotically size-independent, and therefore $ZT \propto N^{1-\xi} = N^{2/3}$.

In Fig. 2, we show, for a given ΔT and different system sizes, the relative efficiency η/η_C as a function of the normalized power P/P_{\max} . Note that these curves have two branches as they are obtained by changing $\Delta\mu$ from zero (where $P = 0$) up to the stopping value, where again $P = 0$, since the electrochemical potential difference becomes too high to be overcome by the temperature difference. In between, power first increases, up to $P = P_{\max}$, and then decreases, leading to a two-branch curve. In the same figure, we also show the analytical result from linear response [12]:

$$\frac{\eta}{\eta_C} = \frac{\frac{P}{P_{\max}}}{2 \left(1 + \frac{2}{ZT} \mp \sqrt{1 - \frac{P}{P_{\max}}} \right)}, \quad (9)$$

where the figure of merit ZT and $P_{\max} = S^2\sigma(\Delta T)^2/(4N)$, derived from Eq. (6) and (7), have been computed previously (see Fig. 1). In spite of the not so small value of $\Delta T/T = 0.2$, there is a good agreement between the results of our numerical simulations and

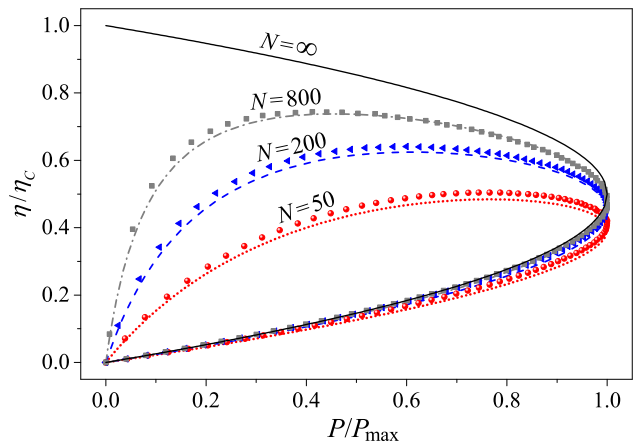


FIG. 2. Relative efficiency η/η_C versus normalized power P/P_{\max} for $\Delta T = 0.2$ ($T_L = 1.1$, $T_R = 0.9$) and different system sizes. The dotted, dashed, dot-dashed curves show the expectation from linear response, Eq. (9), at the $ZT(N)$ value corresponding to the given system size N . The solid line is Eq. (9) for $ZT = \infty$, corresponding to $N = \infty$ in our model. The upper branch of this curve sets the linear-response upper bound on efficiency for a given power.

the universal linear response behavior given by Eq. (9). Moreover, such agreement improves with increasing the system size, as expected since $|\nabla T| = \Delta T/N$ decreases when N increases. For any given ΔT , we expect the linear response to correctly describe the transport properties of our model for large enough system sizes. In Fig. 2, we also show the parabolic curve corresponding to Eq. (9) for $ZT = \infty$ (obtained in our model in the thermodynamic limit $N \rightarrow \infty$), whose upper branch is the universal linear response upper bound to efficiency for a given power P . The expansion of such curve for $P/P_{\max} \ll 1$ leads to

$$\eta(P) \leq \eta_r(P) = \eta_C \left(1 - \frac{1}{4} \frac{P}{P_{\max}} \right), \quad (10)$$

which sets a much less restrictive bound for efficiency-power trade-off than the bound (5) obtained above for non-interacting systems. Our above reported numerical results strongly suggest that the linear-response bound is saturated by our model in the *thermodynamic limit*.

To illustrate the breaking of bound (5) for *finite* system sizes, we compute the maximum efficiency η_{\max} and the corresponding power $P(\eta_{\max})$, for different system sizes. The obtained results, shown as black-white circles in Fig. 3, are in agreement with the linear response predictions, obtained from Eq. (9) at different values of ZT (red circles). For $ZT \rightarrow \infty$ (obtained when $N \rightarrow \infty$), $\eta_{\max} \rightarrow \eta_C$ and $P(\eta_{\max}) \rightarrow 0$. In the limit of large ZT , from Eq. (9) we obtain

$$\eta_{\max} = \eta_C \left(1 - \frac{1}{2} \frac{P(\eta_{\max})}{P_{\max}} \right). \quad (11)$$

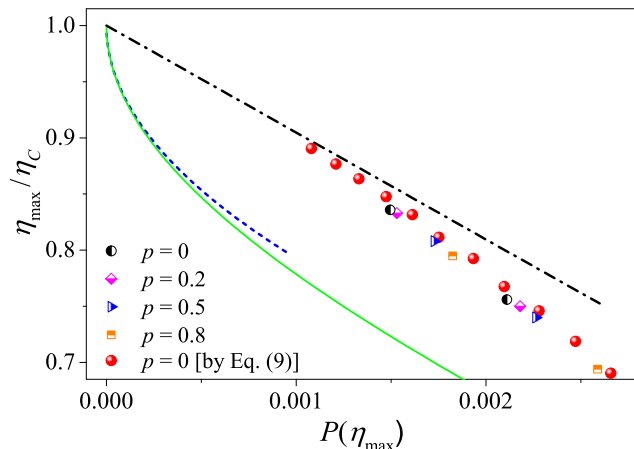


FIG. 3. Maximum efficiency η_{\max} versus the corresponding power $P(\eta_{\max})$, from linear response with the values of ZT obtained numerically (red circles) and directly from numerical computation of power and efficiency (black and white circles) for various system sizes with $T_L = 1.1$ and $T_R = 0.9$. The dot-dashed line is for the analytical expectation from linear response at large ZT , Eq. (11). We also show the bound for classical non-interacting systems (solid line) and its approximation at the low power limit given by Eq. (5) (dashed line) as a comparison. Data from the stochastic model described in the text, with p collision probability each time two particles meet, are also reported (for further details on this model, see Sec. A in the supplementary material).

This power-efficiency trade-off when approaching the Carnot efficiency is much more favorable than the bound for non-interacting systems, also shown for comparison in Fig. 3. To investigate the dependence of power and efficiency on the interaction strength, we introduce a parameter p as follows: When two particles meet, they pass through each other with probability p , while they collide elastically with probability $1 - p$. For our original hard-point model $p = 0$, while for the noninteracting case $p = 1$. We can see in Fig. 3 that data at different values of p stay on a single curve, as expected from linear response. While for a given system size by decreasing interactions (i.e., by increasing p) we reduce ZT and therefore deteriorate the performance of energy conversion, ZT still grows with the system size. In short, the larger p the larger the system size is required to have a given number of collisions per particle crossing the system. Only in the non-interacting case we obtain $ZT = 1$ ($\eta/\eta_C \approx 0.17$) for all system sizes [23].

Conclusions and discussion. In this letter, we have shown that classical interacting systems allow, for a given power, a much higher efficiency than the one achievable in the non-interacting case. This result shows that interactions can significantly improve the performance of heat to work conversion. Our results are based on the fact that for momentum-conserving systems the Carnot efficiency can be achieved at the thermodynamic limit

without delta-energy filtering. While we have considered for illustrative purposes a one-dimensional, diatomic disordered chain of hard-point elastically colliding particles, our theoretical considerations can be as well extended to other momentum-conserving systems, also of higher dimensions [26, 27]. In the non-interacting case, for d -dimensional systems connected to reservoirs via openings of linear size l_α , the injection rate of particles from reservoir α to the system is proportional to $(l_\alpha/\lambda_\alpha)^{d-1}$, and therefore the maximum power scales linearly with this quantity, which plays the role of the number of transverse modes in a classical context. The corresponding non-interacting bound on efficiency at a given power is broken by momentum-conserving systems, as shown in the supplementary material, Sec. D, for the two-dimensional multi-particle collision model [28]. Finally, we have also considered refrigeration (see again the supplementary material, Sec. E) and shown that, thanks to interactions, one can greatly exceed the bound on efficiency for a given cooling power which applies to systems described by the scattering theory. While we conjecture that our results also apply in the quantum case for systems with momentum conservation, such extension remains as a challenging task for future investigations.

Besides their fundamental interest, our findings for momentum-conserving systems could be of practical relevance in situations where the elastic mean free path of the conducting particles is much longer than the length scale over which interactions are effective in exchanging momenta between the particles, as it might happen in high-mobility two-dimensional electron gases at low temperatures. Moreover, our results might find applications in the context of cold atoms, where a thermoelectric heat engine has already been demonstrated for weakly interacting particles [29]. More recent experimental results on coupled particle and heat transport through a quantum point contact connecting two reservoirs of interacting Fermi gases have shown a strong violation of the Wiedemann-Franz law which could not be explained by the Landauer-Büttiker scattering theory [30]. It can be envisaged that in such systems, which can be considered as thermoelectric devices with high efficiency [30], the non-interacting bound on efficiency for a given (cooling) power could be outperformed, with possible applications to the refrigeration of atomic gases.

Supplementary material

Numerical study of efficiency and power

The efficiency and the power of the illustrating one-dimensional (1D) diatomic hard-point chain model have been thoroughly investigated by molecular dynamics simulations. The setup consists of two reservoirs at temperature $T_L = T + \Delta T/2$ and $T_R = T - \Delta T/2$ and electro-

chemical potential $\mu_L = \mu - \Delta\mu/2$ and $\mu_R = \mu + \Delta\mu/2$ (with $\Delta T > 0$ and $\Delta\mu > 0$), respectively, applied to the system at the two ends. The system length, L , is set to be equal to the averaged particle number, N , in the system; therefore in the following we refer to the system size by L or N equivalently. Initially, the system is evolved till it relaxes to the stationary state, then the time averaged particle current J_ρ and energy current J_u are evaluated by evolving the system further. Finally, the power and efficiency are obtained by definition: $P = \Delta\mu J_\rho$ and $\eta = P/J_{h,L}$, where $J_{h,L} = J_u - \mu_L J_\rho$ is the heat current flows from the left (hotter) reservoir. As an illustration, the first column in Fig. 4 shows the typical results.

Note that our model is interacting and nonintegrable. If particles do not interact, i.e., when two particles meet they simply pass through each other without collision, then the system becomes integrable. In order to reveal how the efficiency and the power depend on the interaction strength – which is our main motivation for this work – we introduce a probability, p , that controls the latter and study the dependence of η and P on it [31]. This parameter controls the interaction strength in such a way: when the two particles meet, they have the chance p to pass through each other and the chance $1-p$ to collide elastically. For our original hard-point model $p = 0$, while for the noninteracting, integrable case $p = 1$. For intermediate values of p ($0 < p < 1$) the dynamics is stochastic. As Fig. 4 shows, when the interaction increases (p decreases), both the efficiency and the power increase. In particular, in the range of weak interaction the increasing is remarkably fast. When p decreases to about 0.5, the increasing almost stops and the values of η and P are close to their saturated values at $p = 0$. These results clearly show the important role interactions play in thermoelectric performance.

We have also studied thoroughly the dependence of efficiency and power on the system size N . We find that for $p < 1$, for given ΔT and $\Delta\mu$, both η and P increase with N , which is consistent with the fact that the figure of merit ZT increases with N and agrees with our theoretical predictions for an interacting system (see Fig. 1 and Fig. 2 in the paper for the case $p = 0$). But for the noninteracting, integrable case $p = 1$, as both J_ρ and J_u are independent of the system size, η and P do not depend on N either. In this case ZT can be shown to be an N -independent constant ($ZT = 1$) [23].

Numerical method for evaluating the figure of merit ZT

Numerically, it is a challenge to evaluate the figure of merit ZT in a momentum conserving system when the system size is large. This is also the challenge we encounter for the present study. To overcome this difficulty, we have developed a general, efficient numerical method

that we will outline here. We start from the linear response equations

$$\begin{pmatrix} J_\rho \\ J_u \end{pmatrix} = \begin{pmatrix} L_{\rho\rho} & L_{\rho u} \\ L_{u\rho} & L_{uu} \end{pmatrix} \begin{pmatrix} -\nabla\alpha \\ \nabla\beta \end{pmatrix}, \quad (12)$$

where $\alpha \equiv \beta\mu$. In the literature, the standard method to determine the Onsager coefficients [18, 19, 23] is as follows: First, we set $\Delta\alpha = \Delta$ and $\Delta\beta = 0$, then we can obtain $L_{\rho\rho} = -J_\rho N/\Delta$ and $L_{u\rho} = -J_u N/\Delta$ by calculating the currents J_ρ and J_u in the simulation. After that, we set $\Delta\alpha = 0$ and $\Delta\beta = \Delta$ instead, then we can get $L_{\rho u} = J_\rho N/\Delta$ and $L_{uu} = J_u N/\Delta$ in the same way. Based on these Onsager coefficients, we can derive the transport coefficients σ , κ , and S , and finally the thermoelectric figure of merit ZT . This method (hereafter referred to as method A) requires that Δ is small enough to obtain results independent of Δ , as expected for the linear response. We find that σ and S do not depend on Δ sensitively, while the problem arises in computation of thermal conductivity

$$\kappa = \frac{1}{T^2} \left(L_{uu} - \frac{L_{\rho u} L_{u\rho}}{L_{\rho\rho}} \right), \quad (13)$$

as in this case we need to compute a quantity which scales as $\sim N^{1/3}$ from the difference of two quantities, L_{uu} and $L_{\rho u} L_{u\rho}/L_{\rho\rho}$, which scale linearly with the system size due to the momentum is conserved [23]. For a given Δ , the error in such quantities also scales linearly with N , and therefore with method A it is possible to measure κ accurately only if we take $\Delta \sim 1/N$. This implies prohibitive costs in the simulations for large N .

To solve this problem, we have developed a different method (referred to as method B) that allows us to compute κ accurately for a fixed Δ at any value of N . Since the heat conductivity is computed at zero particle flow, the key point is to find values $(\Delta\alpha, \Delta\beta)$, or equivalently $(\Delta T, \Delta\mu)$, which ensure $J_\rho = 0$. Our method is as follows:

- For a given value of ΔT , set $T_L = T + \Delta T/2$ and $T_R = T - \Delta T/2$. Then calculate J_ρ and J_u by simulations as a function of $\Delta\mu$ with $\mu_L = \mu - \Delta\mu/2$ and $\mu_R = \mu + \Delta\mu/2$;
- Based on the function $J_\rho(\Delta\mu)$, determine $\Delta\mu^*$ such that $J_\rho(\Delta\mu^*) = 0$, then the heat conductivity is evaluated from the relation

$$J_u(\Delta\mu^*) = -\kappa\nabla T = \kappa\Delta T/N. \quad (14)$$

Figure 5 shows the typical dependence of J_ρ and J_u on $\Delta\mu$. Interpolating the data points for J_ρ we can determine $\Delta\mu^*$ from the condition $J_\rho(\Delta\mu^*) = 0$ and then evaluate $J_u(\Delta\mu^*)$ and κ as explained above. Note that the interpolation procedure can be iterated to obtain more accurate value of $\Delta\mu^*$ and consequently of κ .

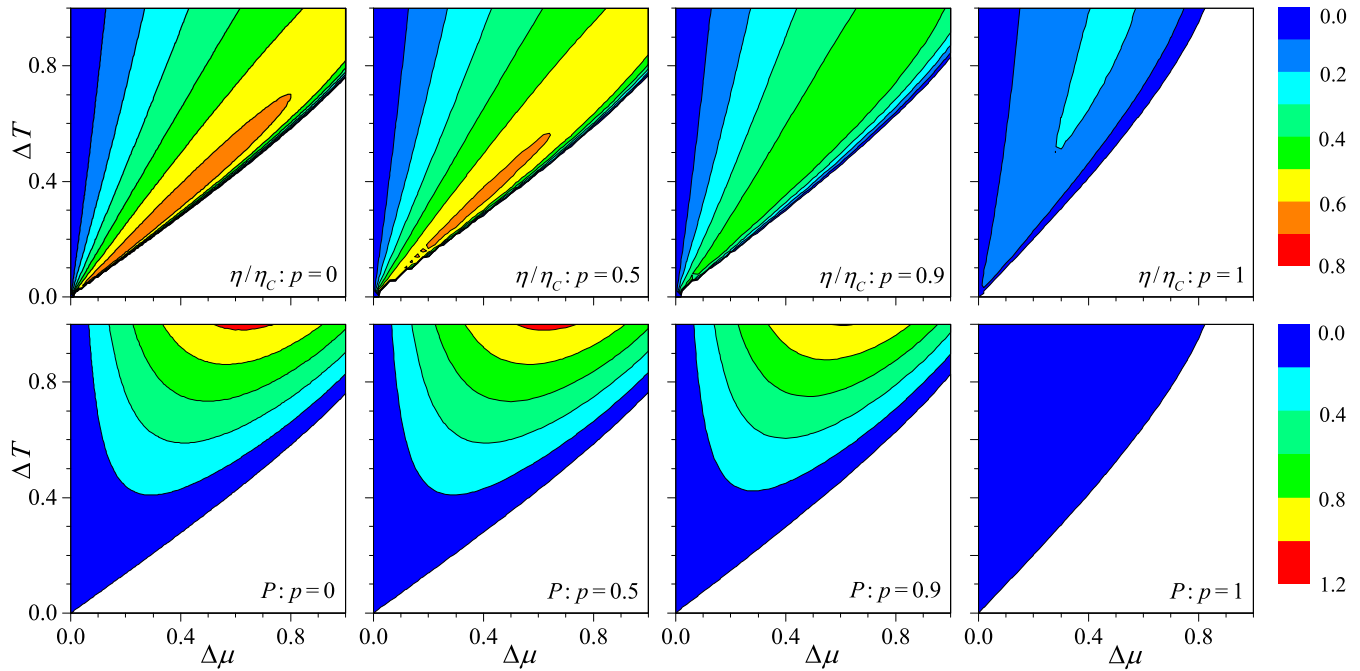


FIG. 4. The numerically obtained efficiency (normalized to the Carnot efficiency, upper row) and the power (lower row) as a function of the temperature difference ΔT and the electrochemical potential difference $\Delta\mu$ between two applied reservoirs for the hard-point diatomic chain model (first column) and its variants parameterized by a non-zero p (from the second to the forth column) for $T = 1$, $\mu = 0$, and $L = N = 200$. The parameter p introduces a stochastic element in the systems's dynamics: when two particles meet, they may (with a probability p) pass through each other instead of colliding. All four panels in each row are plotted with the same scale indicated at the end. In the white area of each panel the power is negative, and therefore the system cannot be used for power production.

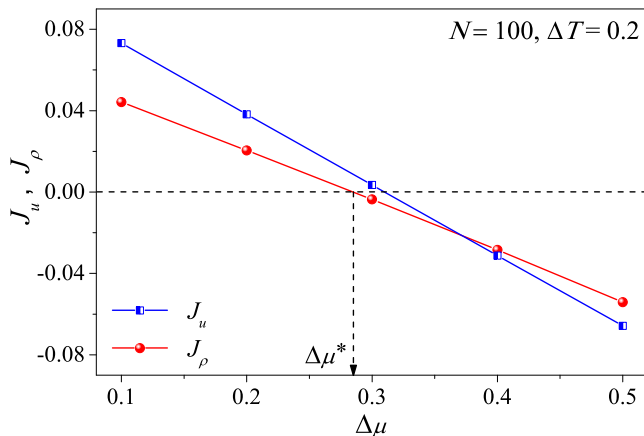


FIG. 5. Particle and energy current as a function of $\Delta\mu$ for a given ΔT in the hard-point diatomic chain model.

We finally compare in Fig. 6 method B for two given values of ΔT with method A at different values of Δ . The results of method A coincide with those of method B, provided Δ is taken smaller and smaller when N increases. This shows that method B is reliable and suitable to obtain accurate results for the thermal conductivity at large

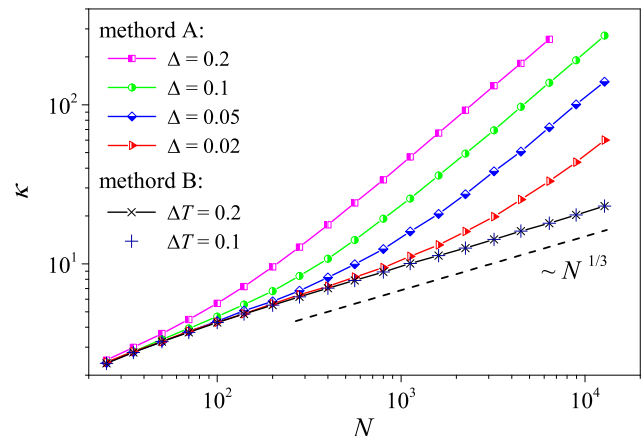


FIG. 6. Comparison of the standard method used in the literature for computing the heat conductivity (method A) with that we have developed (methods B).

system sizes (in Fig. 6 up to $N = 12800$).

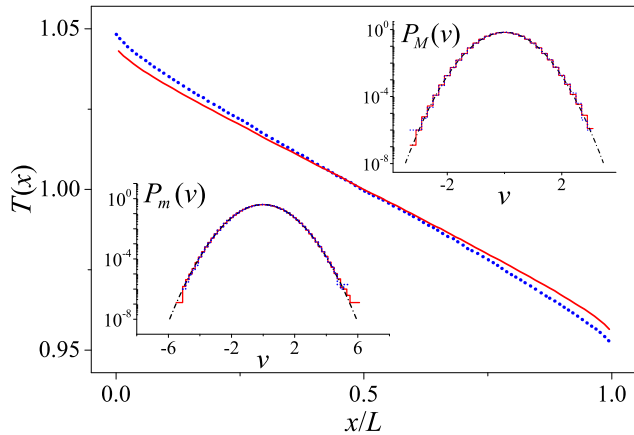


FIG. 7. The temperature profile of the steady state (main panel) and the velocity distributions of the two species of particles at the middle point $x = L/2$ (insets) of the diatomic chain system with $m = 1$ and $M = 3$. In the main panel and the insets, the red solid (blue dotted) line is for $L = N = 100$ (800). The black dash-dotted line in the insets are for the Boltzmann distribution for mass m and M , respectively, with the evaluated temperature $T(x) = 1$. Note that the three lines in each inset agree with each other so well that it is difficult to distinguish them.

Energy distribution

For a thermoelectric system that can be modelled by the scattering theory, the Carnot efficiency can be achieved for delta-energy filtering, i.e., when only carriers within a given energy window are allowed to transmit through the system, and the width of such window tends to zero [15–17]. It is therefore interesting to investigate if this mechanism also works in our diatomic chain model [31]: Does the energy distribution in the system shrink as the system size increases?

To this end, we study the velocity distributions of the two species of particles, $P_m(v)$ and $P_M(v)$, when they pass a given position, x , in the system. We find that they always agree perfectly with the Boltzmann distribution at a local temperature $T(x)$ for $m \neq M$. Indeed, due to interactions, our system always relaxes to a steady state and reaches the local equilibrium, and this property does not depend on the system size. Therefore the mechanism for the Carnot efficiency is approached in our system is fundamentally different from the delta-energy filtering.

As an example, in Fig. 7 the velocity distributions and the temperature profiles at two different system sizes, $L = N = 100$ and 800, are presented and compared. The temperatures and the electrochemical potentials of the reservoirs are $T_L = 1.05$, $T_R = 0.95$, $\mu_L = -\Delta\mu^*/2$, and $\mu_R = \Delta\mu^*/2$, respectively, with $\Delta\mu^* = 0.143$ (0.148) for $N = 100$ (800). The system is evolved till it relaxes to the steady state, then the velocity distributions along

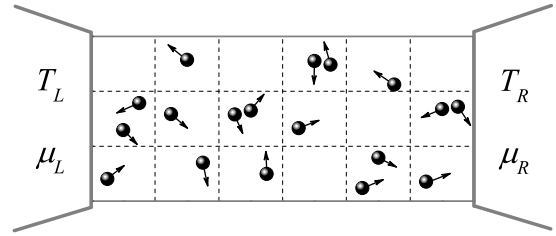


FIG. 8. Schematic plot of the 2D momentum-conserving gas of interacting particles, described by the multi-particle collision dynamics. The cells of dashed-line boundaries represent the partition of space considered for modeling collisions.

the system are calculated. The simulation results suggest convincingly that $\langle \frac{1}{2}mv^2 \rangle = \langle \frac{1}{2}Mv^2 \rangle$ at any position x , which implies the local equilibrium. The temperature can therefore be defined and obtained by identifying the averaged energy to $\frac{1}{2}k_B T(x)$.

The insets of Fig. 7 show the velocity distributions at the middle point $x = L/2$ of the system, and they all fully agree with the Boltzmann distribution of temperature $T(x) = 1$. At other places the velocity distributions are also the same as the Boltzmann distribution with a certain temperature, which is evaluated and presented in the main panel. Note that the temperatures at the left and right ends of the system are slightly different from the external temperatures T_L and T_R . This boundary effect, which is the result of a boundary (Kapitza) resistance, vanishes as the system size increases.

An additional illustrating example: The 2D momentum-conserving gas of interacting particles

For non-integrable momentum-conserving systems, our theory is general. To show its generality and in particular its independence of dimensionality, here we provide another illustrating example. The model system we consider is a two-dimensional (2D) momentum-conserving gas of interacting particles (see Fig. 8 for a schematic plot). All particles have the same mass m , and we set $m = 1$. The length of the system is L ; two reservoirs are coupled at the two ends. The width of the system, i.e., its size in the transverse direction, is l , and in this direction the periodic boundary condition is applied.

The evolution of the system is described by the multi-particle collision (MPC) dynamics [28], introduced as a stochastic model to study solvent dynamics. Collisions are modelled by coarse graining the time and space at which interactions occur, and hence simplifies the numerical simulations of interacting particles. By MPC, the system evolves in discrete time steps, consisting of free propagation during a time τ followed by instantaneous

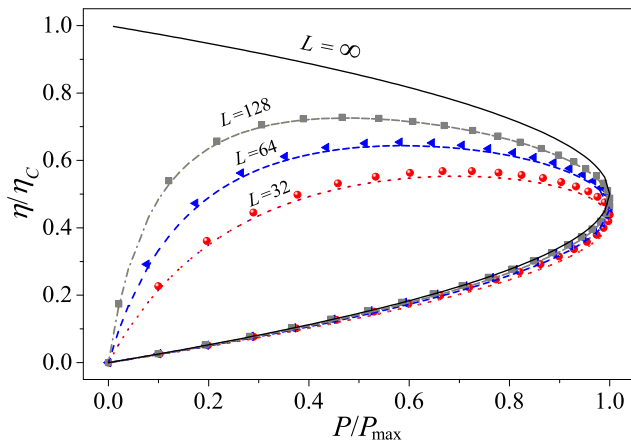


FIG. 9. Relative efficiency η/η_C versus normalized power P/P_{\max} for various system length L of the 2D gas model. The dotted, dashed, dot-dashed curves show the expectation from the linear response analysis, Eq. (9) in the main paper, at the $ZT(L)$ value corresponding to the system length L . The solid line is Eq. (9) for $ZT = \infty$, corresponding to $L = \infty$. The upper branch of this curve sets the linear response upper bound on efficiency for a given power.

collision events. During the free propagation period, a particle keeps its velocity \mathbf{v}_i unchanged but changes its position from \mathbf{r}_i to $\mathbf{r}_i + \tau\mathbf{v}_i$. For the collisions, the system is partitioned into identical square cells of side a (see Fig. 8), then the velocities of all particles found in the same cell are rotated with respect to their center of mass velocity \mathbf{V}_{CM} by two angles, α or $-\alpha$, randomly chosen with equal probability. The velocity of a particle in the cell is thus updated from \mathbf{v}_i to $\mathbf{V}_{CM} + \hat{R}^{\pm\alpha}(\mathbf{v}_i - \mathbf{V}_{CM})$, where $\hat{R}^{\pm\theta}$ is the 2D rotation operator of angle θ .

Note that the MPC dynamics keeps the total momentum and energy conserved. By using our new numerical method (see Sec. B), we checked that in this model ZT diverges as the system size increases [32]. As our linear response analysis is independent of the system's dimension, it is expected that the thermoelectric power-efficiency trade-off follows the theoretical prediction Eq. (9) and the asymptotic relation Eq. (11) given in the main paper.

To verify this conjecture, thorough numerical simulations are carried out for various values of the system length L . Other parameters adopted are as follows: $T_L = 1.1$, $T_R = 0.9$, $l = 2$, $a = 0.1$, $\alpha = \pi/2$, and the averaged particle number density $\rho = 22.75$. The reference electrochemical potential is set to be $\mu = 0$ for the adopted value of ρ at temperature $T = 1$. For each given L value, we take $\mu_L = -\Delta\mu/2$ and $\mu_R = \Delta\mu/2$ and investigate how the thermoelectric power and efficiency depend on $\Delta\mu$. The results are presented in Fig. 9; it can be seen that the simulation results agree with the linear-response theoretical prediction very well.

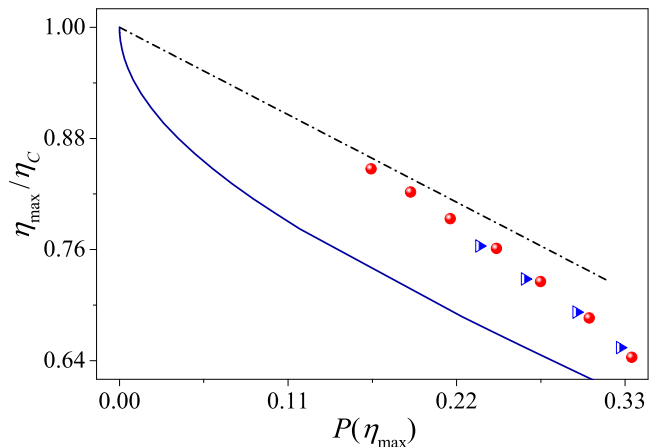


FIG. 10. Maximum efficiency η_{\max} versus the corresponding power $P(\eta_{\max})$ of the 2D gas model, evaluated from the linear response theory [Eq. (9) in the paper] with the simulated Onsager coefficients (red dots) and directly from numerical computation of power and efficiency (blue triangles) for various system sizes. The dot-dashed line is for the analytical expectation from linear response at large ZT , Eq. (11) in the paper. For comparison, the bound for 2D classical non-interacting systems (solid line) with $T_L = 1.1$, $T_R = 0.9$, and $\rho = 22.75$ is also given.

In Fig. 10, we summarize the results for the maximum efficiency versus the corresponding power for various L , obtained via direct simulations (blue triangles) and via the theoretical result [Eq. (9) in the paper] with ZT and P_{\max} computed from the numerically simulated Onsager coefficients (red dots). It can be seen that results obtained with the two methods agree with each other and consistently approach the theoretical prediction [Eq. (11) in the paper] for large ZT . Importantly, in this figure we can see that the thermoelectric efficiency at a given power of this interacting system outperforms the 2D non-interacting bound, which we are going to derive below.

For the 2D non-interacting systems, the maximum efficiency for a given power can be obtained following the same steps as in the 1D case. The particle reservoirs are modelled as 2D ideal gas systems. The velocity distribution inside the ideal gas reservoirs is the Maxwell distribution. Particles enter from reservoir α into the system through an opening of length l , with an injection rate γ_α (for a short description of this effusion process, see Appendix B in [12]). The particle current is given by

$$J_\rho = \gamma_L \int_0^\infty d\epsilon u_L(\epsilon) \mathcal{T}(\epsilon) - \gamma_R \int_0^\infty d\epsilon u_R(\epsilon) \mathcal{T}(\epsilon), \quad (15)$$

where $\mathcal{T}(\epsilon)$ is the transmission probability for a particle with energy ϵ to transit from one end to the other end of the system, $0 \leq \mathcal{T}(\epsilon) \leq 1$. The injection rate from

reservoir α is given by

$$\gamma_\alpha = \frac{l\rho_\alpha}{\sqrt{2\pi m\beta_\alpha}}, \quad (16)$$

and the energy distribution of the injected particles is

$$u_\alpha(\epsilon) = 2\beta_\alpha e^{-\epsilon\beta_\alpha} \sqrt{\frac{\epsilon\beta_\alpha}{\pi}}. \quad (17)$$

We can then express the density and the injection rate in terms of the electrochemical potential and of the de Broglie thermal wave length $\lambda_\alpha = h/\sqrt{2\pi m k_B T_\alpha}$ (m is the mass of the injected particles and h the Planck constant) as

$$\mu_\alpha = k_B T_\alpha \ln(\lambda_\alpha^d \rho_\alpha), \quad (18)$$

where d is the dimensionality of the reservoirs and of the system (in our case, $d = 2$). Therefore

$$\gamma_\alpha = \frac{e^{\beta_\alpha \mu_\alpha}}{h\beta_\alpha} \left(\frac{l}{\lambda_\alpha}\right)^{d-1}. \quad (19)$$

We finally obtain that

$$J_\rho = \frac{2\sqrt{2ml}}{h^2} \int_0^\infty d\epsilon \sqrt{\epsilon} [f_L(\epsilon) - f_R(\epsilon)] \mathcal{T}(\epsilon) \quad (20)$$

with $f_\alpha(\epsilon) = e^{-\beta_\alpha(\epsilon - \mu_\alpha)}$. The heat current from reservoir α is similarly obtained as

$$J_{h,\alpha} = \frac{2\sqrt{2ml}}{h^2} \int_0^\infty d\epsilon \sqrt{\epsilon} (\epsilon - \mu_\alpha) [f_L(\epsilon) - f_R(\epsilon)] \mathcal{T}(\epsilon). \quad (21)$$

Starting from Eqs. (20) and (21) for particle and heat currents in two dimensions, one can follow the 1D derivation reported in the main text and obtain the 2D bound from scattering theory for the maximum efficiency at a given power output (shown as the full blue curve in Fig. 10).

We note that the same derivation can be performed also for three-dimensional systems, with in that case, for an opening of area l^2 ,

$$u_\alpha(\epsilon) = \beta_\alpha^2 e^{-\epsilon\beta_\alpha} \epsilon, \quad (22)$$

and

$$\gamma_\alpha u_\alpha(\epsilon) = \frac{2\pi m l^2}{h^3} \epsilon f_\alpha(\epsilon). \quad (23)$$

Overcoming the scattering-theory bound for refrigeration

When a thermoelectric device works as a refrigerator, the most important benchmark is the coefficient of performance (COP)

$$\eta^{(r)} = \frac{J_{h,L}}{P_{\text{abs}}}, \quad (24)$$

given by the ratio of the cooling power $J_{h,L}$, that is, the heat current extracted from the cold reservoir (which without lack of generality we assume to be the left one, i.e., $T_L < T_R$), over the absorbed power P_{abs} . The COP can never exceed Carnot's limit,

$$\eta^{(r)} \leq \eta_C^{(r)} = \left(\frac{T_R}{T_L} - 1\right)^{-1}. \quad (25)$$

With a calculation analogous to the one performed in the main paper for power production, we can compute the maximum COP allowed by nonlinear classical scattering theory for a given cooling power. For 1D systems, we obtain that the optimal transmission function is a boxcar function, $\mathcal{T}(\epsilon) = 1$ for $\epsilon_0 < \epsilon < \epsilon_1$ and $\mathcal{T}(\epsilon) = 0$ otherwise. Differently from power production, here $\epsilon_1 = -\Delta\mu\eta_C^{(r)}$ ($\Delta\mu = \mu_R - \mu_L < 0$) and $\epsilon_0 = -\Delta\mu J'_{h,L}/P'_{\text{abs}}$, where the prime indicates the derivative over $\Delta\mu$ for fixed \mathcal{T} . The maximum cooling power is obtained when $\epsilon_1 \rightarrow \infty$ and is given by

$$(J_{h,L})_{\text{max}}^{(\text{st})} = \frac{k_B^2 T_L^2}{h}. \quad (26)$$

Note that in this case $-\Delta\mu \rightarrow \infty$ as well and therefore the absorbed power $P_{\text{abs}} = -(\Delta\mu)J_\rho \rightarrow \infty$, implying that the COP vanishes. At low cooling power, $J_{h,L} \ll (J_{h,L})_{\text{max}}^{(\text{st})}$, the upper bound on the COP approaches the Carnot's limit as follows:

$$\eta^{(r)} \leq \eta_{\text{max}}^{(r,\text{st})}(J_{h,L}) = \eta_C^{(r)} \left(1 - C \sqrt{\frac{T_R}{T_R - T_L} \frac{J_{h,L}}{(J_{h,L})_{\text{max}}^{(\text{st})}}}\right), \quad (27)$$

with $C \approx 0.813$. The Carnot's limit is obtained for delta-energy filtering, $\epsilon_1 - \epsilon_0 \rightarrow 0$, and in this limit the cooling power vanishes.

Interestingly and importantly, we find that the cooling performance of an interacting system can surpass the bound set by the nonlinear classical scattering theory as well at the large ZT regime. By a linear response analysis [12], the maximum COP is

$$\eta_{\text{max}}^{(r)} = \eta_C^{(r)} \frac{\sqrt{ZT + 1} - 1}{\sqrt{ZT + 1} + 1}, \quad (28)$$

which is reached at the cooling power

$$J_{h,L} = \frac{\Delta T}{L} \sqrt{\kappa(\kappa + S^2\sigma T)}, \quad (29)$$

where $\Delta T = T_R - T_L > 0$ and L is the system length. At the low-power limit, it is approximated by

$$\eta_{\text{max}}^{(r)} \approx \eta_C^{(r)} \left(1 - \frac{2L J_{h,L}}{S^2 \sigma T \Delta T}\right). \quad (30)$$

As here $\eta_{\text{max}}^{(r)}$ is a linear function of $J_{h,L}$, this bound is, in the high-efficiency region, higher than that of the nonlinear classical scattering theory, Eq. (27).

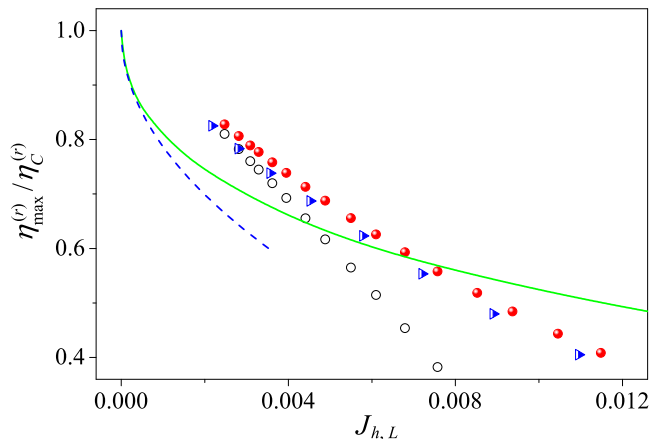


FIG. 11. The cooling performance of the 1D hard-core, diatomic gas model for various system sizes with $T_L = 0.975$ and $T_R = 1.025$. The full red dots are for the linear response prediction [Eq. (28)-(29)] and the open circles are for its low-power approximation [Eq. (30)]. The blue triangles are for the direct simulation results. For these three sets of data points, the system size and ZT increases from right to left. The upper bound predicted by the nonlinear classical scattering theory and its low-power approximation [Eq. (27)] are shown by the solid green line and the blue dashed line, respectively.

In order to make a comparison of the two theoretical predictions, we take the 1D diatomic, hard-core interacting gas again as an illustrating example. We assume that two particles will not pass through each other when they collide (i.e., $p = 0$) and the electrochemical potential at the studied state of $T = 1$ and particle density $\rho = N/L = 1$ is zero. The masses of particles are $m = 1$ and $M = 3$. First, by using the new numerical method described in Sec. B, we calculate the transport coefficients and ZT at the studied state for various system sizes. Then the dependence of the COP on the cooling power given by the linear response analysis [Eq. (28)-(29)] and its low-power approximation [Eq. (30)] are evaluated. The results for $T_L = 0.975$ and $T_R = 1.025$ are presented in Fig. 11. It can be seen that the maximum efficiency of the system for a given cooling power becomes higher than the bound of Eq. (27) for noninteracting systems when $J_{h,L} < 0.006$.

In Fig. (11), the cooling performance measured in direct simulations for various system sizes is also presented and the results corroborate our linear response analysis convincingly. In our simulations for a given system size, the system is coupled to two reservoirs at temperature T_L and T_R and at electrochemical potential $\mu_L = 0$ and $\mu_R = \Delta\mu$, respectively. For a given value of $\Delta\mu$, the cooling power and the efficiency are measured in the stationary state. Then by changing $\Delta\mu$, the cooling power and the efficiency as a function of $\Delta\mu$ are obtained, based on which the maximum efficiency and the corresponding

cooling power are in turn identified.

Our analysis of refrigeration can be extended to two and three dimension straightforwardly. For the 2D interacting gas with the MPC dynamics (see Sec. D), we have obtained qualitatively the same results.

Acknowledgments: We are grateful to Dario Poletti for fruitful discussions and to an anonymous referee for useful suggestions. We acknowledge support by NSFC (Grants No. 11535011 and No. 11335006) and by the INFN through the project QUANTUM.

-
- [1] F. Giazotto, T. T. Heikkilä, A. Luukanen, A. M. Savin, and J. P. Pekola, *Rev. Mod. Phys.* **78**, 217 (2006).
 - [2] A. Shakouri, *Annu. Rev. Mater. Res.* **41**, 399 (2011).
 - [3] Y. Dubi and M. Di Ventra, *Rev. Mod. Phys.* **83**, 131 (2011).
 - [4] M. Campisi, P. Hänggi, and P. Talkner, *Rev. Mod. Phys.* **83**, 771 (2011).
 - [5] J. T. Muhonen, M. Meschke, and J. P. Pekola, *Rep. Prog. Phys.* **75**, 046501 (2012).
 - [6] U. Seifert, *Rep. Prog. Phys.* **75**, 126001 (2012).
 - [7] R. Kosloff, *Entropy* **15**, 2100 (2013).
 - [8] B. Sothmann, R. Sánchez, and A. N. Jordan, *Nanotechnology* **26**, 032001 (2015).
 - [9] D. Gelbwaser-Klimovsky, W. Niedenzu, and G. Kurizki, *Adv. At. Mol. Opt. Phys.* **64**, 329 (2015).
 - [10] G. Benenti, G. Casati, C. Mejía-Monasterio, and M. Peyrard, *From thermal rectifiers to thermoelectric devices*, in *Thermal transport in low dimensions*, S. Lepri (Ed.), *Lecture Notes in Physics* **921** (Springer, 2016).
 - [11] S. Vinjanampathy and J. Anders, *Contemporary Physics* **57**, 1 (2016).
 - [12] G. Benenti, G. Casati, K. Saito, and R. S. Whitney, *Phys. Rep.* **694**, 1 (2017).
 - [13] R. S. Whitney, *Phys. Rev. Lett.* **112**, 130601 (2014).
 - [14] R. S. Whitney, *Phys. Rev. B* **91**, 115425 (2015).
 - [15] G. D. Mahan and J. O. Sofo, *Proc. Natl. Acad. Sci. USA* **93**, 7436 (1996).
 - [16] T. E. Humphrey, R. Newbury, R. P. Taylor, and H. Linke, *Phys. Rev. Lett.* **89**, 116801 (2002).
 - [17] T. E. Humphrey and H. Linke, *Phys. Rev. Lett.* **94**, 096601 (2005).
 - [18] C. Mejía-Monasterio, H. Larralde, and F. Leyvraz, *Phys. Rev. Lett.* **86**, 5417 (2001).
 - [19] H. Larralde, F. Leyvraz, and C. Mejía-Monasterio, *J. Stat. Phys.* **113**, 197 (2003).
 - [20] K. Saito, G. Benenti, and G. Casati, *Chem. Phys.* **375**, 508 (2010).
 - [21] H. B. Callen, *Thermodynamics and an Introduction to Thermostatistics* (2nd ed.) (John Wiley & Sons, New York, 1985).
 - [22] S. R. de Groot and P. Mazur, *Nonequilibrium Thermodynamics* (North-Holland, Amsterdam, 1962).
 - [23] G. Benenti, G. Casati, and J. Wang, *Phys. Rev. Lett.* **110**, 070604 (2013).
 - [24] S. Lepri, R. Livi, and A. Politi, *Phys. Rep.* **377**, 1 (2003).
 - [25] A. Dhar, *Adv. Phys.* **57**, 457 (2008).
 - [26] G. Benenti, G. Casati, and C. Mejía-Monasterio, *New J. Phys.* **16**, 015014 (2014).

- [27] S. Chen, J. Wang, G. Casati, and G. Benenti, Phys. Rev. E **92**, 032139 (2015).
- [28] A. Malevanets and R. Kapral, J. Chem. Phys. **110**, 8605 (1990).
- [29] J.-P. Brantut, C. Grenier, J. Meineke, D. Stadler, S. Krinner, C. Kollath, T. Esslinger, and A. Georges, Science **342**, 713 (2013).
- [30] D. Husmann, M. Lebrat, S. Häusler, J.-P. Brantut, L. Corman, and T. Esslinger, preprint arXiv:1803.00935 [cond-mat.quant-gas].
- [31] We thank an anonymous referee for suggesting this study to us.
- [32] This result was first pointed out by G. Benenti, G. Casati, and C. Mejía-Monasterio, New J. Phys **16**, 015014 (2014).